Citation: Lian, Mengying, Sun, Jiaxin, Jiang, Dawei, Xu, Miaojun, Wu, Zijian, Xu, Bin, Algadi, Hassan, Huang, Mina and Guo, Zhanhu (2023) Waterwheel-inspired high-performance hybrid electromagnetic-triboelectric nanogenerators based on fluid pipeline energy harvesting for power supply systems and data monitoring. Nanotechnology, 34 (2). 025401. ISSN 0957-4484

Published by: IOP Publishing

URL: https://doi.org/10.1088/1361-6528/ac97f1 <https://doi.org/10.1088/1361-6528/ac97f1>

# Waterwheel-inspired high-performance hybrid electromagnetic-triboelectric nanogenerators based on fluid pipeline energy harvesting for power supply systems and data monitoring

Mengying Lian[a], Jiaxin Sun[a], Dawei Jiang[a]*, Miaojun Xu[a], Zijian Wu[b], Ben Bin Xu[c], Hassan Algadi[d], Mina Huang[e,f], Zhanhu Guo[f]*

[a]Mengying Lian, Jiaxin Sun, Dawei Jiang*, Miaojun Xu
College of Chemistry, Chemical Engineering and Resource Utilization, Northeast Forestry Univer-sity, Harbin 150040, P. R. China
Dawei Jiang
E-mail: daweijiang@nefu.edu.cn
[b]Zijian Wu
Key Laboratory of Engineering Dielectrics and Its Application, Ministry of Education, Harbin Uni-versity of Science and Technology, Harbin 150040, P. R. China
[c]Ben Bin Xu
Department of Mechanical and Construction Engineering, Faculty of Engineering and Environment, Northumbria University, Newcastle upon Tyne, NE1 8ST, UK
[d]Hassan Algadi
Department of Electrical Engineering, Faculty of Engineering, Najran University, P.O. Box 1988, Najran 11001, Kingdom of Saudi Arabia
[e]Mina Huang
College of Materials Science and Engineering, Taiyuan University of Science and Technology, Taiyuan, 030024, China
[f]Zhanhu Guo
Integrated Composites Laboratory (ICL), Department of Chemical and Biomolecular Engineering, University of Tennessee, 1512 Middle Dr, Knoxville, TN, 37996, USA
Zhanhu Guo
E-mail: nanomaterials2000@gmail.com

**Abstract:** In this work, a self-powered system based on a triboelectric-electromagnetic hybrid pipeline energy harvesting module is demonstrated. Rabbit fur and poly tetra fluoroethylene (PTFE) are used as triboelectric electrodes to fabricate disk-type soft-contact triboelectric nanogenerators (TENGs) instead of traditional direct-contact TENGs to collect the mechanical energy of water flow and convert it into electrical energy. This design has a stable electrical output and gives an improved durability. Its simple fabrication process enables excellent potential for practical applications in industry. In addition, the hybridization of electromagnetic generator (EMG) module and TENGs module to form a triboelectric-electromagnetic hybrid nanogenerator (TEHNG) can improve the electrical output performance, especially the current output. TEHNG can not only power small electronic devices, such as lighting systems, but also collect independent fluid energy and monitor data signals simultaneously in harsh environments, such as fluid energy harvesting in industrial production pipelines and temperature and humidity in fluid environments. This work provides an efficient strategy to harvest multiple energies simultaneously, significantly increasing the yield and promoting the application of TENGs in engineering.

**Keywords:** Triboelectric nanogenerator; Magnetic coupling; Fluid energy; Power supply system; Data monitoring

## 1. Introduction

Artificial intelligence (AI) and computers are the symbol of modern society, and the efficient use of various resources is an inevitable factor. In terms of energy, the nuclear energy [1], solar energy [2] and wind energy [3, 4] have been required by the city. In addition, human movement energy [5], vibration energy [6] and other energy are gradually utilized, which can be collected for small equipment. The widespread use of distributed energy has attracted worldwide attention [7-10]. Triboelectric nanogenerator (TENGs) is a device that collects environmental mechanical energy and generates electric energy by combining triboelectric effect and electrostatic induction. The piezoelectric nanogenerator (PENG) is a device that uses the piezoelectric effect of special nanomaterials to convert mechanical energy into electric energy when subjected to an external stretching or compression. Both nanogenerators could convert mechanical energy into electricity. PENGs could effectively harvest various weak mechanical energies in the environment and use them to drive electronic devices, which is of great value for the deployment of mobile sensor networks [11]. However, compared with PENGs, TENGs could effectively convert irregular, distributed, and wasted mechanical energy into electricity. Other advantages include the lower cost, simpler structure, lighter weight, and higher efficiency [12, 13]. In addition, the principle of TENGs is based on the coupling of triboelectric and electrostatic induction, with higher electrical properties such as voltage and electrical power [14, 15]. TENGs are now likely to be used in sensors [16, 17], artificial intelligence [18, 19], biomedicine [20], and blue energy [21, 22] due to their extremely low cost, lightweight design, and combination of diverse materials and functions. Furthermore, TENGs could even replace conventional battery supplies to power implantable [23] or wearable devices [24, 25]. In order to fully exploit and utilize the advantages of TENGs self-driving energy for various systems or devices, more extensive and in-depth research is imperative. Compared with other types of TENGs devices, rotary triboelectric nanogenerators (R-TENGs) are more efficient, durable, and efficient [26, 27]. An R-TENGs aimed at harvesting tiny wind energy was developed based on the coupling effect of triboelectric and electrostatic induction [28]. By introducing polymer nanowires to the surface of the friction electrode, it directly drives nearly a hundred light-emitting diodes (LEDs) and is used as a self-powered sensor for measuring the wind speed [29-31]. However, as the running time of the R-TENGs increases, the friction time of the friction electrodes accumulates and the frictional heat generation affects the performance of the R-TENGs equipment, the power generation efficiency of the machine is affected, and the power output is poor [32, 33]. Therefore, non-contact (NC)-RTENGs and R-TENGs with automatic mode switching (AMT) between contact and non-contact modes were invented. A new configuration to generate electricity by moving between electrodes after charge generation induction was fabricated, and this NC-TENGs could generate electricity in a universally applicable manner via electrostatic induction [34, 35]. For NC-TENGs, the wear between the triboelectric electrodes is avoided, but the accumulated charges on the surface of the dielectric layer are also relatively reduced. A super-stable AMT-rotating TENGs via automatic mode switching with electrical output performance was realized by charging excitation, with electrical output performance much higher than that of normal contact TENGs [36, 37]. For AMT-type TENGs, the friction loss of the dielectric layer still exists, and the long-term operation will also reduce the electrical output performance of the TENGs. The R-TENGs based on fur or soft friction layer as a flexible dielectric layer reduces the influence of the mutual friction between the dielectric layers on the power output of the R-TENGs and is called a fur-rotation triboelectric nanogenerator (FR-TENGs), which has high stability, high durability and high voltage output performance.

Numerous power generation-based capabilities make TENGs useful for many applications. However, the characteristics of high voltage output, low current and low power make TENGs have limitations in practical applications. In order to make up for the shortcomings of TENGs in terms of current and power output, researchers have tried to use solar cells [38], PENGs [39, 40], or EMGs [41, 42] to hybridize TENGs to address the above challenges. Among them, the hybrid generator of TENGs and EMG has been proved to be a reliable way to obtain electricity. Self-monitoring systems are required to close the technology gap, which includes triboelectric inertial module capabilities and electromagnetic systems [43, 44]. An excellent circular design, according to the triboelectric-electromagnetic working principle, is to establish an excellent battery monitoring system. This work not only provided an efficient and sustainable way to find blue energy, but also demonstrated the strong application potential of TENGs to the complexity of marine resources. A well-established TEHNG hydroelectric collector had been developed [45]. A free triboelectric layer-mode TENGs was fabricated using ribbon magnet silicon material and nylon film-bonded electrodes as triboelectric materials, which were then electrically bonded to the electrodes. The hybrid generator was a simply coupled TENGs cylinder with an EMG by an oscillating structure designed for ultra-low frequency power [46, 47]. The device provided an impressive 0.1 Hz water conversion efficiency with a maximum power of 10.16 W $m^{-3}$ and an average power of 0.23 W $m^{-3}$. Furthermore, the hybrid nanogenerator (NG) array successfully achieves thermal energy design and continuous heat transfer, demonstrating its ability to accumulate water energy. The magnets and copper coils in most EMG-TENGs modules are fixed on the substrates of the rotor and stator of the disk-TENGs, respectively, and the middle of the EMG is often separated by friction electrodes [48, 49], while the strong magnetic neodymium magnets and copper coils in this work are unblocked, increasing induced currents in copper coils. In addition, TEHNG modules are generally used to collect blue energy [43, 50], wind energy [51], mechanical energy of human movement [52] and heat energy [31, 53], and convert them to electrical energy for the power various devices. However, it is rare for TENGs to collect the mechanical energy of the fluid flowing in the pipeline, and the fluid in the pipeline is abundant in industrial production, so a TEHNG module that utilizes the mechanical energy of pipeline fluid to generate electricity is designed.

Herein, a self-powered system based on a triboelectric-electromagnetic hybrid pipeline energy harvesting module is demonstrated. Rabbit fur and PTFE are used as triboelectric electrodes to fabricate disk-type soft-contact TENGs instead of traditional direct-contact TENGs to collect the mechanical energy of water flow and convert it into electrical energy. This design has stable electrical outputs and improve the durability of TENGs, and its simple fabrication process has excellent potential for practical applications in industry. In addition, the TEHNG consists of an EMG module and a disk-TENGs module within a certain device volume, so the electrical output performance, especially the current output can be improved. Especially through the new module, it is possible to simultaneously collect independent fluid energy and monitor data signals in harsh environments, such as the collection of fluid energy in industrial production pipelines and the monitoring of data such as temperature and humidity in the fluid environment. This work provides an efficient strategy to simultaneously harvest multiple energies, significantly enhancing the output and facilitating the applications of TENGs in engineering (Figure 1).

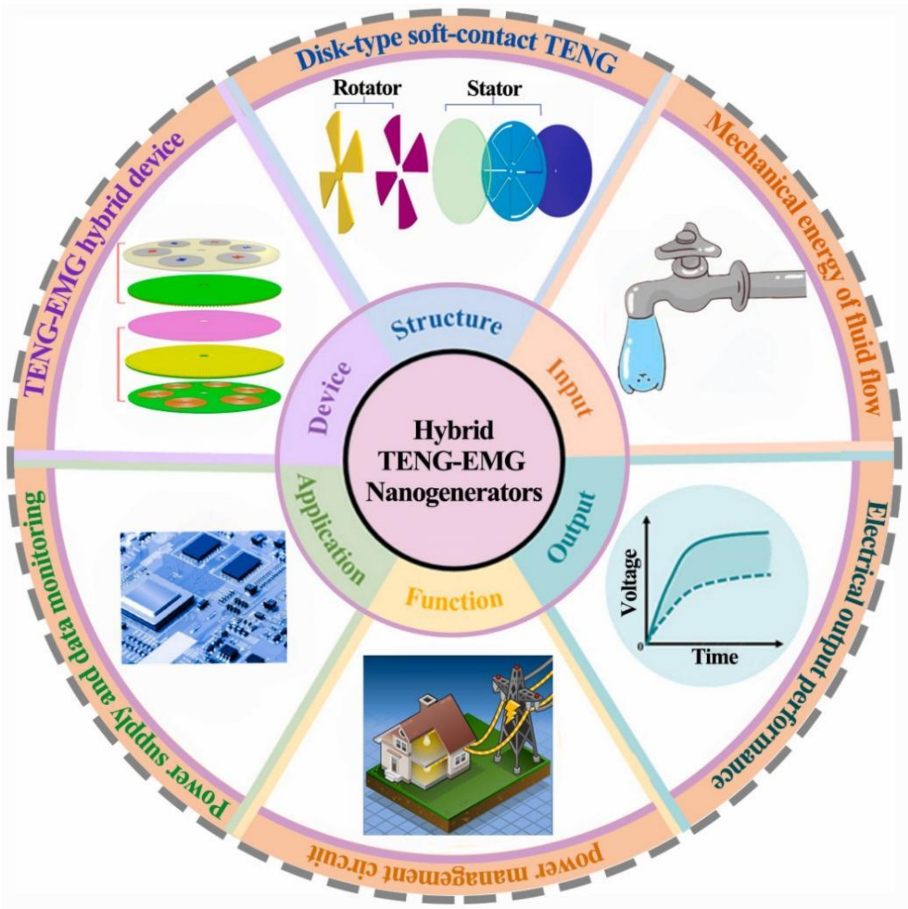


**Figure 1.** Schematic diagram of input energy, structure, device, application, function and electrical output of a hybrid TENGs-EMG nanogenerator driven by fluid flow mechanical energy.

## 2 Results and discussion

### 2.1 Principle of the designed TEHNG

A waterwheel is an irrigation device that can lift water in ancient China. The principle is that when the water pushes the water wheel, the water spoon on the water wheel head will be filled with water (Figure 2i), and then the water in the water spoon is transported to the top of the water wheel and flows into the water channel (Figure 2ii-2iii), the water in the water channel It then flows to the irrigation pipe (Figure 2iv) and into the irrigation field. Inspired by the principle of the inertial rotating water wheel of water, this work invents a hybrid nanogenerator (NG) that harnesses the flow of water in pipes to generate electricity.

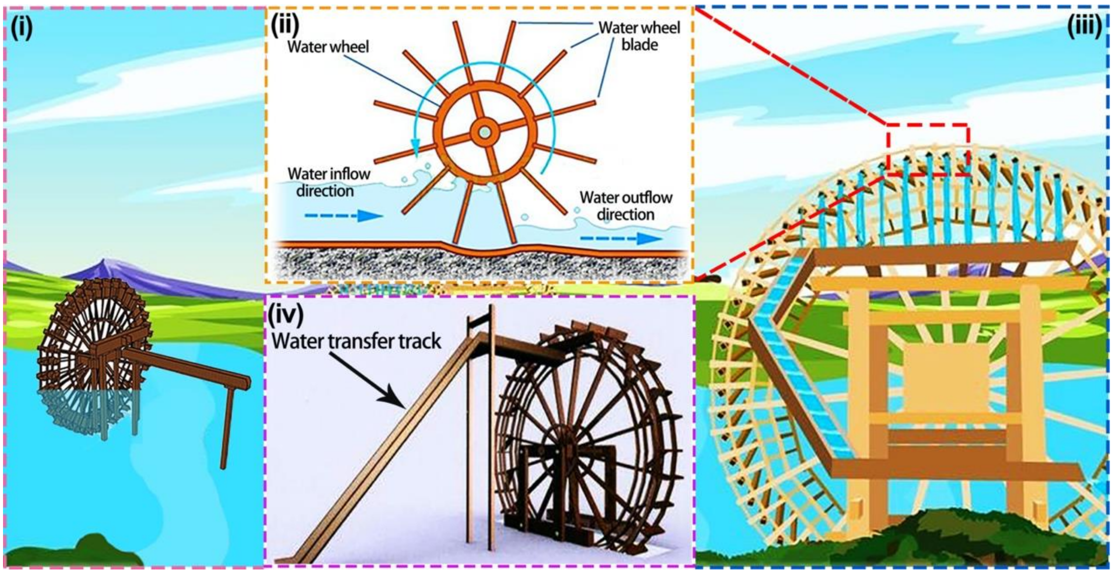


**Figure 2.** Schematic diagram of a waterwheel, i) drawing water from the river with water scoop by the water force, ii) transporting water to a high place, iii) pouring water into the water channel, iv) water flowing to the field.

The triboelectric electrodes of TENGs (such as polymer film and metal) are mainly electrified by contact through sufficient mutual friction to transfer electrons between the two triboelectric electrodes. However, in this case, due to the friction between the contact electrodes and the effect of the large torque in the TENGs, the contact material will be severely damaged and its service life will be shortened. The TENGs module working in soft-contact connection mode can solve these problems. The addition of the fur soft-contact friction electrode module reduces the resistance and loss of the TENGs during the friction process, protects the surface of the friction electrode, and improves the durability of the TENGs. The common direct-contact TENGs use copper electrodes in contact with polymers to triboelectrically electrify, while disk-type soft-contact TENGs are based on the independent contact mode, with triboelectric electrodes composed of animal fur or polyester fibers and polymers. The power generation principle of disk-type soft-contact TENGs is based on triboelectric electrification and electrostatic induction between different materials, and the electric potential difference caused by the contact time difference is used to generate electrical output. When operated under external mechanical pushes, the PTFE dielectric layer and the rabbit fur fans brush contact each other to transfer electrons, creating electrostatic charges on both surfaces until saturation (Figure 3a). The copper friction electrode is manufactured by the printed circuit board (PCB) technology to obtain precise friction electrode size and effective friction area and the manufacturing design of the PCB process is carried out using the altium designer program (Figure 3b). The triboelectric electrification principle of disk-type soft-contact TENGs is shown in Figure 3c. The PTFE adhered to the PCB's surface is used as the stator, the rabbit fur attached to acrylic plate is used as the rotor, and the brushes on the rotor are placed the state above the stator is used as the initial condition (Figure 3c i). Before the rotor starts to rotate, it is assumed that the TENGs has been pre-charged, at which time the rotor is aligned with the triboelectric dielectric layer, and the rabbit fur and PTFE triboelectrodes are in an electrically neutral state. As the rotor rotates, the two friction electrodes of rabbit fur and PTFE are constantly frictioned. Due to electrostatic induction, the charges of the right induction electrode flow to the left copper electrode, and the current flows from the left copper induction electrode to the right until the positive and negative charges cancel each other out (Figure 3c ii-3c iii). Negative charges were induced on the right electrode to prevent positive polarization from passing through it. As the scalloped fur was rotated counterclockwise relative to the stationary electrode (Figure 3c iv), the intensity of positive polarization on the right electrode was decreased but the intensity on the left electrode was increased. When the charge flowing from the right copper induction electrode to the left copper induction electrode reaches a saturation, the short-circuit current flowing through the load is 0, and then the power generation process of the TENGs enters the second half (Figure 3c v). Since there is a potential difference between the left copper electrode and the right copper electrode, the charges on the left copper electrode will flow to the right copper electrode, and the current will flow from the right copper electrode to the left until the electric potential difference between the two copper electrodes is 0 (Figure 3c vi-3c vii). Then due to electrostatic induction, the charge of the left copper electrode flows to the right copper electrode. At this time, the left copper electrode is positively charged, the right copper electrode is negatively charged, and the current flows from the right copper electrode to the left (Figure 3c viii). As a result, the free charges on the two electrodes are redistributed due to the triboelectric electrification and electrostatic induction, and the charges are transferred from the right electrode to the left electrode, thereby generating a current flow from the left electrode to the right electrode in the external circuit. After the rabbit fur friction electrode passes through the entire copper electrode, the charge returns to the right electrode to generate a pulse through an external resistor. Then, the TENGs module enters the next cycle of power generation, and the next power generation principle is the same as that in Figure 3c, resulting in an alternating current. A constant rotation produces a continuous alternating current output of the disk-type soft-contact TENGs. Due to its structural characteristics and the insulating properties of its materials, TENGs usually has a high voltage output, but the current output is relatively poor, and the hybrid NG between EMG and TENGs just makes up for this shortcoming. The schematic diagram of the water turbine installed in the pipeline and the direction of the water flow are shown in Figure 3d. The mechanical energy of the fluid flow promotes the rotation of the water wheel, which causes the magnetic flux through the copper coil to change, generating an electric current. The principle of the EMG part of the hybrid NG is based on Faraday's law of electromagnetic induction, which transfers alternating current through periodic changes in the magnetic flux in the coil. Figure 3e depicts a schematic diagram of an EMG operating in one third of a cycle. In the initial state, the unnotched magnet is aligned with the coil, and under the action of the positive magnetic field, there is no current in the coil (Figure 3e i). When the water wheel rotates 45 degrees clockwise to reach the Figure 3e ii state, the magnetic flux of the copper coil gradually decreases, and the first-stage induced current is generated due to the change of the magnetic flux in the coil. When the turbine continues to rotate, the coil has an opposite magnetic field due to the increase in the magnetic flux, and at the same time, generates an induced current opposite to the second stage (Figure 3e iii). When the turbine continues to rotate, the magnetic flux passing through the copper coil reaches the maximum, no longer changes, and reaches a new state equivalent to the initial state, so the induced current is no longer generated (Figure 3e iv). The change in current during the rotation of the turbine as described above indicates that the EMG has an alternate output current/voltage.

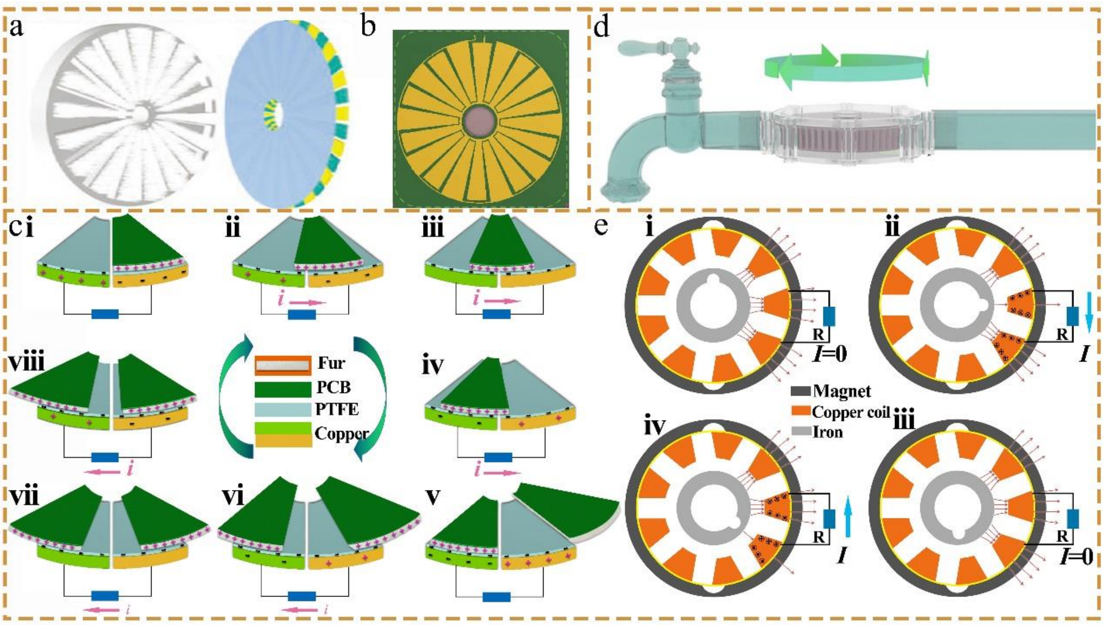


**Figure 3.** Fabrication schematics and schematics of TENGs and EMG. **a)** Structure diagram of disk soft-contact TENGs. **b)** Schematic diagram of PCB triboelectrode. **c)** Schematic of disk soft-contact TENGs. **d)** Schematic diagram of water turbine installed on a water pipe. **e)** Schematic of EMG.

### 2.2 Electrical characterizations for the disk soft-contact TENGs

The output voltages of disk-TENGs with PTFE triboelectric electrodes and copper induction electrodes with different grating numbers were investigated, and the disk-TENGs with different grating numbers contributed significantly to the current. The test system was driven by a motor rotating at 1200 rpm (Figure 4a). Subsequently, different grating numbers are arranged for the disk soft-contact TENGs to test its electrical output performance. The outputs of voltage and current of different grating numbers have large differences, while the output of the amount of charge has almost no difference. In order to reveal the effect of the induction electrodes of different grating numbers on the performance of the charge amount, the charges of the TENGs in the 6 to16 grating numbers are almost equal with the prolongation of the friction time between rabbit fur and PTFE. After the transfer number of charges is accumulated for a long enough time, since the surface areas of the induction electrodes in different grating numbers are the same, the charges transfer on the surface of the dielectric layer will eventually reach the same state after different times (Figure 4b). In addition, due to the wobble of the TENGs caused by the high-speed rotation, the poor contact between the rabbit fur and the dielectric layer resulted in a slight difference in the value of the output charges. Figure 4c illustrates the voltage output characteristics of different segmented structures. With increasing the number of TENGs gratings, the output trend of the voltage decreases gradually. When the grating number is 8, the voltage reaches a maximum value of 5.3 kV. This is attributed to the fact that the number of triboelectric charges decreases with the increase of the gratings, the triboelectric dielectric layer is attached by the PTFE film, and the frictional area of each grating decreases with the increase of the gratings, thus resulting in a decrease in the potential difference. Due to some errors in the experimental process, the TENGs voltage value of 6-gratings is smaller than the voltage value of 8-gratings. The TENGs's currents in different gratings were measured, and as the induction electrode gratings became denser, the current increased from 0.1 μA to about 1 μA. The output short-circuit current of TENGs can be increased by increasing the charge transfer frequency. Similarly, the current can be increased by increasing the number of gratings, with a TENGs of 16 gratings reaching 1 μA when driven externally at 1200 rpm. A faster relative motion of the two triboelectric electrodes of TENGs means a faster charge transfer and higher average output power. Therefore, increasing the relative motion is an effective way to improve the electrical performance of TENGs, so we introduce motors to drive the electrodes and fur to rotate in different directions. As the gratings increase, the speed of charges transfer gradually increases, and the generation of current depends on the transfer of charges, which will lead to an increase in current, which can be explained by $I=dQ/dt$. The output of the electrical properties of disk-TENGs is essentially a process in which there is a potential difference between two adjacent copper induction electrodes due to time difference, and charges are transferred between adjacent copper induction electrodes, thereby forming a current. Therefore, when the grating number of the copper electrode and the two friction electrodes increases, the charges transfer time decreases, the current transfer rate increases, and the current increases significantly (Figure 4d). The power output performance when loaded with resistors was also characterized, with peak current-resistance and peak power-resistance relationships shown in Figure 4e-f, supporting information. The instantaneous output power is calculated by:

$$P = I_t^2 R \tag{1}$$

where $R$ is the load resistance and $I_t$ is the instantaneous current across the resistance. In addition, the electric power of the TENGs of the induction electrodes in different gratings is compared, and the current of the TENGs with 8 gratings is obviously the smallest, so the value of its electrical power is also the smallest. With the increase of the gratings, the output current gradually increases and its electric power will also increase. We enumerate the electrical power output performance of other TENGs with different gratings in the supporting literature Figure S1. The maximum power of TENGs in different gratings is almost $10^4$ times the minimum power, which provides a basis for us to study the performance and potential applications of TENGs in different gratings.

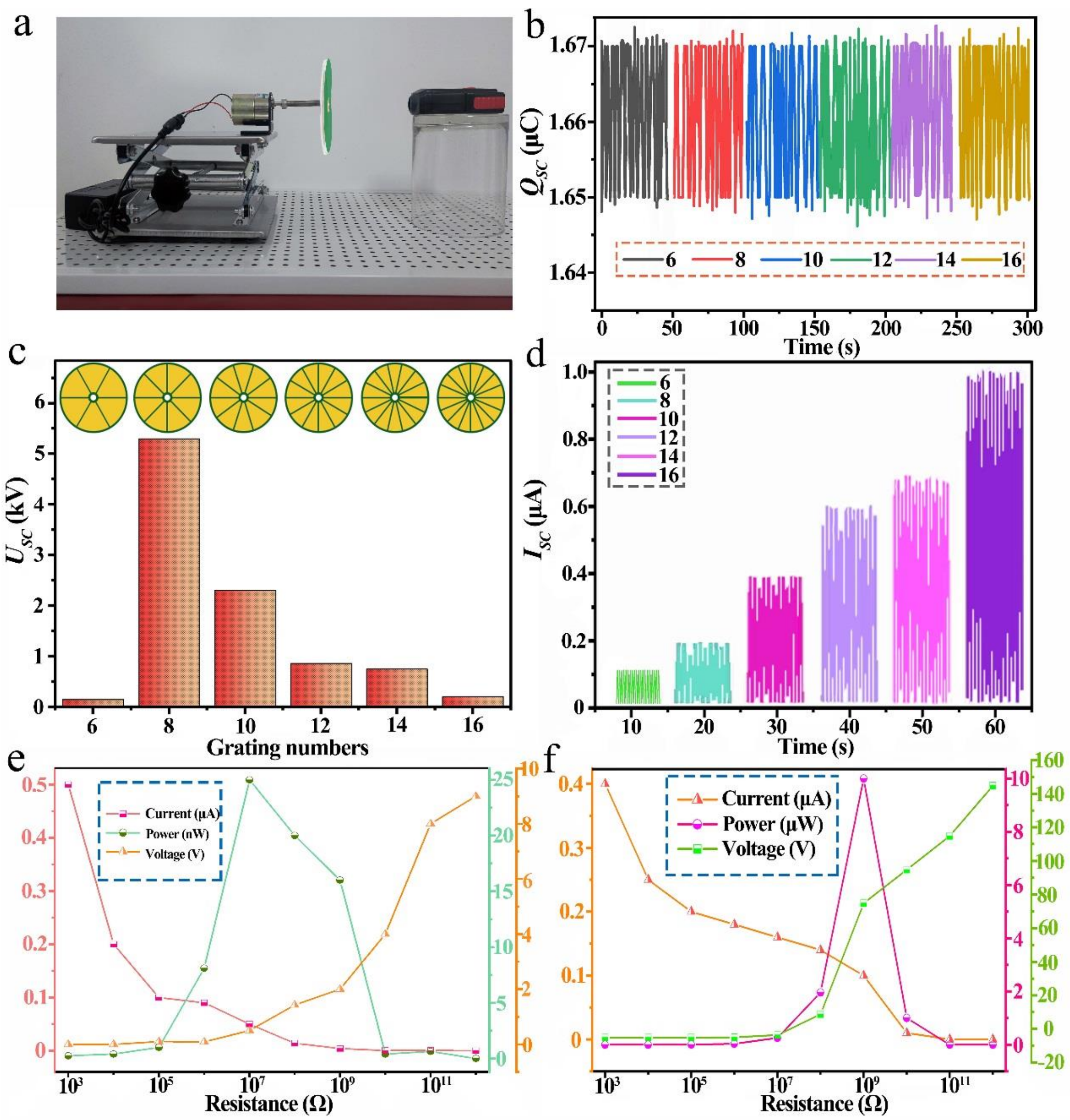


**Figure 4.** Disk-type soft-contact TENGs electrical output performance in different gratings. **a)** TENGs electrical output test device. **b-d)** Output performance of charges, voltage and current amount of TENGs in different gratings. **e)** Power performance of 8-gratings TENGs. **f)** Power performance of 16-gratings TENGs.

To investigate the effect of fur type on the electrical output performance of TENGs, some common animal furs and polyester (polyester fibers) obtained from rabbits, sheep, dogs and foxes were selected for comparison. A standard dynamic rotational speed measurement system was established to study the relationship between the frictional rotational speed of various fur triboelectric materials and the output of TENGs (Figure 5a). The TENGs was placed on the optical table, and the rotating disc fur friction electrode was fixed on the motor by a dynamic torque sensor, which was used to measure the effect of rotational speed on the electrical output of the TENGs in real time. The motor and dynamic torque sensor are mounted on the optical table, and the central axis is kept in the same line. During measurement, real-time speed and torque can be displayed on the display. The TENGs made of fur discs with different animal furs and polyester fibers was used as the rotor, and the ordinary PTFE film for comparison was used as the dielectric layer with the speed of 1200 rpm. Figure 5b-c and Figure S2 show the transferred charge, output short circuit current and short circuit voltage of TENGs and the electrical output performance of several common animal fur and polyester fibers as impervious friction materials. The distribution of rabbit fur fibers is a complex and it could be divided into straight needle fur and fluff. The straight needle fur is long and thick without curling, the fluff is relatively short and fine, and very soft. However, the distribution of dog fur, wool and fox fur fibers belongs to the bundle type, which is relatively coarse and long in length. In addition, the friction coefficient of rabbit fur fiber is smaller than that of other three kinds of fur, mainly due to the diameter of the straight needle fur of rabbit is much smaller than that of other three kinds of fur. Rabbit fur TENGs exhibited the highest output performance of 1260 nC, 28 μA, and 3750 V among the four TENGs (Figure 5b-c; Figure S2, Supporting Information), which is related to the high fur density and softness of rabbit fur. The ability to bind extranuclear electrons of PTFE is stronger than that of fur, so during the friction process, the atoms in the fur lose extranuclear electrons and are charged with positive charges, while the rubber rods gain electrons and are charged with negative charges. Because in the During the friction process, according to the law of conservation of charge, only the charge is transferred from one object to another, so the amount of negative charge on PTFE should be equal to the amount of positive charge on fur. The protruding parts of the polymer surface, which are damaged by shear during the friction process, together with the thermal effect of the contact area, form a hot zone. In the hot zone, the polymer will plasticize and melt, resulting in polymer chain breakage and cracking. In the cold region, the polymer is more prone to brittle fracture, and homolytic fracture will generate some free radicals. The ions and free radicals formed by the fragmentation of polymer segments have high energy, instability, and short lifespan, and these active particles quickly proceed to the next step. In the process of friction between PTFE and rabbit fur, homolytic cleavage of low-polarity carbon-carbon bonds in the polymer chain dominates, generating hydrocarbon free radicals and fluorocarbon free radicals. Since PTFE is electronegative, rabbit fur is electropositive, electrons will be transferred from hydrocarbon chain radicals to fluorocarbon chain radicals, thus forming a positively charged hydrocarbon chain and a negatively charged fluorocarbon chain, so that PTFE is generally negatively charged, and rabbit fur is generally positively charged. Before being subjected to external force, the triboelectric pair is independent and neutral. Furthermore, if there is no difference in potential between the two electrodes, no change in charge will be created and caused. When the two triboelectric layers PTFE and rabbit fur are in contact with each other, the same amount of surface charge is transferred in the contact area due to the triboelectric effect. Since dog fur, fox fur, wool, rabbit fur and polyester fiber have the highest density of rabbit fur and the most fluffy and soft texture, its electrical output performance is also the largest, and the amount of point load transfer, The values of voltage and current are 1.6 μC, 5.1 kV and 1.0 μA respectively. In particular, it should be noted that at medium speed, that is, when the water flow rate is close to the water flow rate of the domestic water pipeline, the electrical properties of the rabbit fur TENGs and the polyester fiber TENGs differ by the greatest multiples, which further illustrates the use of rabbit fur as the friction material feasibility and practicality. In addition, environmental factors other than TENGs's own structure have a great influence on its electrical output performance. For the disk soft-contact TENGs, its electrical output varies with the rotation speed of the two triboelectric electrodes. The maximum values of short-circuit voltage and short-circuit current are significantly increased from 200 rpm to 1200 rpm. The increase of the short-circuit current is caused by the high-speed rotation of the TENGs. According to the formula $I=dQ/dt$, when the rotation speed increases, the frequency of charges transfering from one copper electrode to the other side increases, and the charging speed increases linearly with the rotation speed, and the current increases. In general, the output voltage does not depend on the rotation speed of the TENGs and can maintain a constant voltage. However, due to the less instability of the motor, the TENGs rotor obtains a larger rotational torque. With the increase of rotational speed and rotational torque, the contact between the PTFE film and the rabbit fur became more and more closely.

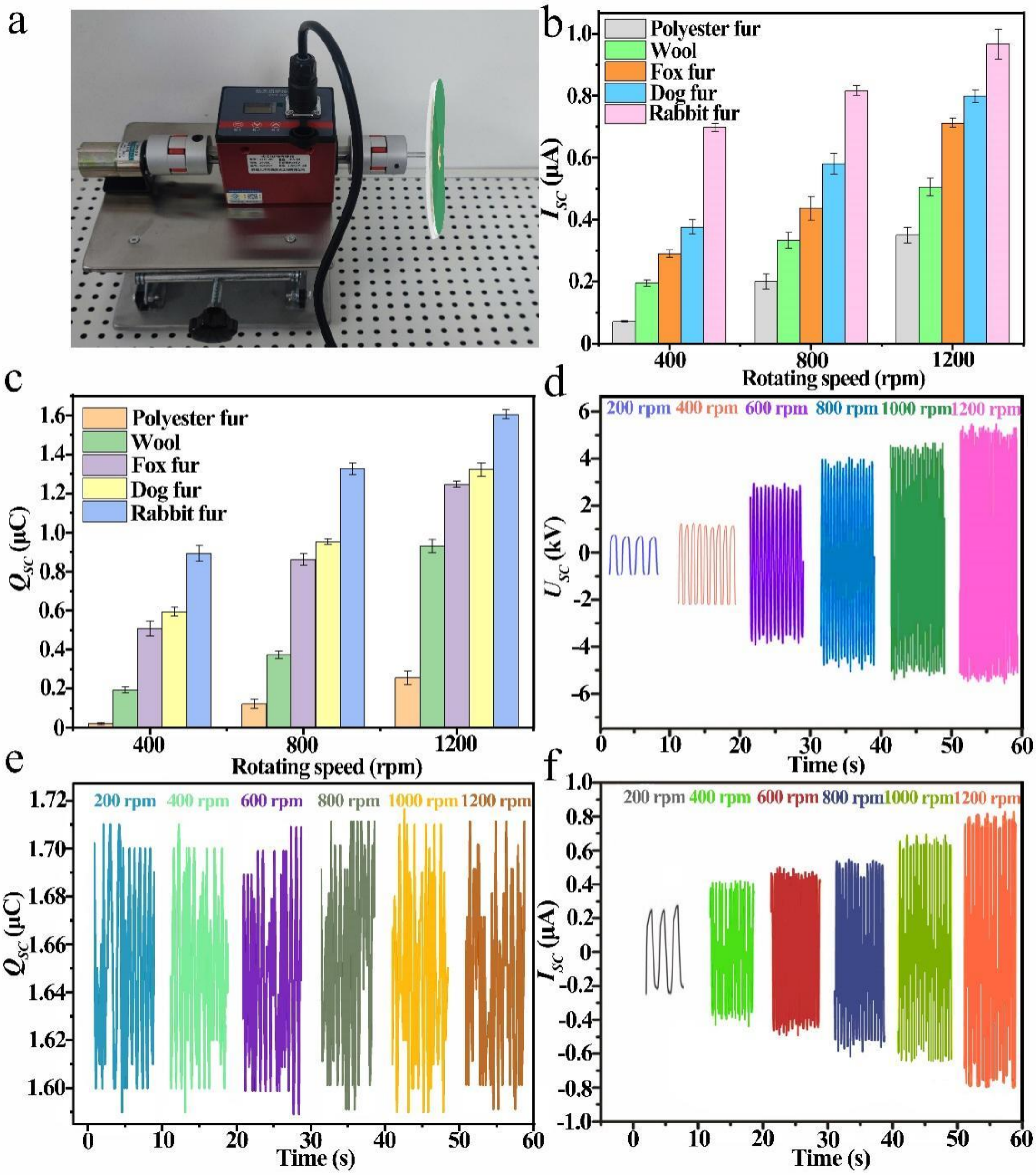


**Figure 5.** The electrical output performance of TENGs under the conditions of different fur as friction electrodes and different rotational speeds. **a)** Picture of the test system. **b-c)** Electrical output performance of TENGs as triboelectrode with different fur. **d-f)** Electrical output performance of TENGs with rabbit fur triboelectrode at different rotational speeds.

Due to the soft texture of rabbit fur, it becomes dense as the number of friction increases, so that the contact area between it and PTFE will increase with the increase of the number of friction times. In addition, it is not excluded that there will be a breakdown voltage between the two friction electrodes, which may also be one of the reasons for the increase of the short-circuit voltage with the increase of the rotational speed. The short-circuit charge depends on the contact area of the two friction electrodes. When the grating numbers of PTFE take a certain value, the size of the contact area between each grating and the rabbit fur is certain, and the amount of charge transferred due to friction electrification is also a certain value. In practice, the maximum output power is usually achieved by combining the TENGs with the best possible output. Therefore, the output performance of TENGs can be improved by matching the optimal performance under external load conditions. The value of the charge transfer amount of the TENGs under different rotational speed conditions is almost the same over time, because the area of the TENGs is exactly the same and the amount will be almost the same (Figure 5d-f).

### 2.3 Electrical characterizations for the TEHNG

When harvesting mechanical energy, since the power density of TENGs is sometimes relatively low, and the friction effect is weakened with the accumulation of friction times, better strategies are needed to improve the power generation efficiency. The general method is to combine the TENGs module with the EMG module, and the non-coupling force between the two modules converts the externally input mechanical energy into electrical energy through these two modules. For example, a rotating TENGs in parallel with an independent EMG is an excellent strategy. Therefore, the combined output of these two components can easily capture a wide range of energy. Figure 6a is a picture of TEHNG installed in a tap water pipeline, which has been shown to have a good effect on reducing material wear and improving energy conversion efficiency. The flow of liquid in the pipeline will drive the turbine and

TENGs to rotate together, thereby converting the mechanical energy of the fluid flow into effective electrical output. The neodymium magnet fixed on the rotating water wheel rotates through the flow of fluid in the pipeline. When a part of the conductor of the closed circuit cuts the magnetic field line in the magnetic field, the magnetic flux will also change, and current will be generated in the conductor. In addition, we studied the electrical output performance of the hybrid NG and found that its charges transfer amount is not much different from that of TENGs, as shown in Figure 6b, because the charges transfer amount of EMG is related to the change of magnetic flux in the coil loop, which can be obtained from the following equation illustrate:

$$Q=I\Delta t=\frac{n\Delta\Phi}{R} \tag{2}$$

where n is the number of turns in the coil, $\Delta\Phi$ is the change in magnetic flux, and R is the resistance of the coil. To demonstrate the better electrical output performance of the hybrid NG and the feasibility of mixing EMG with TENGs, the electrical output performance of TEHNG and TENGs was compared (Figure 6c and Figure S3, Supporting Information). We mixed the EMG module with TENGs, and compared the output current of TEHNG and TENGs at the same rotational speed, and found that the output current of TEHNG was 150 times different than that of TENGs, which was attributed to the high current and stable characteristics of the EMG module. When the EMG module is not added, the maximum current output of the TENGs is less than 1 μA, while the current of the hybrid generator is as high as 0.14 mA, a considerable change in the order of magnitude. In addition, the change in the voltage of the hybrid NG is not much different from that of TENGs, so adding EMG has little effect on the voltage. In practice, combining a TEHNG with suitable resistors gives the maximum power output, so the performance of the TEHNG can be improved by finding the best way to have different resistors than the external load. The peak power can be calculated as formula (1), because it is equivalent to the Joule heat of the resistor, where $I_t$ and $R$ are the current on the applied load and the resistance of the load resistor, respectively. As shown in Figure 6d, the output current of the TEHNG decreased with the increase of the load resistance at 1200 rpm, however, the peak value of the power increased, and when the load resistance was set to $10^7$ Ω, the maximum peak power was 1.6 mW. This is a thousand-fold increase compared to the maximum output power of 1.6 μW without the addition of the EMG module, and the electrical output performance and the applicable range have substantially changed, thanks to the addition of EMG, which makes the current of the hybrid generator very high boost. Figure 6e shows the charging voltage curves of different sizes of commercial capacitors powered by a hybrid NG consisting of TENGs module and EMG module. At the same time, by adding the optimized structure design of the EMG module, the measured voltage of capacitors with different specifications can be charged to its maximum value through the TEHNG module, and the charging rate is inversely proportional to its capacity the smaller the specification, the faster the charging rate. The maximum charging voltage of the capacitor is 12 V, the charging time is the shortest, and the 10 nF capacitor has the longest time. The comparison of voltage, current and electric power of other NGs and TEHNG modules in this work is listed in Table 1. The voltage of TEHNG in this work is significantly higher than that of other NGs, which is attributed to the large amount of charge transfer during the friction between the rabbit fur of disk soft-contact TENGs and PTFE. In addition, the working current of this work also reaches 0.14 mA, which is obviously superior to other devices. Although the power is slightly inferior in value due to experimental errors, it can power 7 W lamps in practical applications, which is equivalent to hundreds of times the power of other NGs.

**Table 1.** Comparison of electrical output performance of this TEHNG with previous modules.

| | Voltage (V) | Current (μA) | Power (mW) | Ref. |
|---|---|---|---|---|
| Waterwheel hybrid generator | 92.65 | 8.64 | 1.75 | [49] |
| Windmill-like hybrid NG | 1150 | 670 | 4.35 | [54] |
| Hybrid biofuel NG | 22 | 10.5 | 13.2 | [55] |
| Honeycomb-structured TENGs | 1207 | 68.5 | 12.4 | [56] |
| Polarization-controlled hybrid NG | 180 | 53 | 0.127 | [57] |
| This work | 5300 | 140 | 6 | |

The electrical output performance of the hybrid NG module has been tested, and then we tested the electrical output performance of TEHNG in practical applications, and tested its electrical output performance under different water pressure conditions in the pipeline. In addition, external environmental influence factors such as environment also have a great influence on the output performance of TEHNG. For TEHNG rotation mode, the output performance depends on the rotation speed. The most direct indicator of piping is fluid pressure. The electrical output performance of TENGs is related to its rotational speed, and the output voltage and current increase with the rotational speed. As shown in Figure 6f, when the pressure of the pipeline increases from 0.1 MPa to 0.35 MPa, the peak values of short-circuit current and open-circuit voltage increase linearly. Large short-circuit currents are caused by high-speed rotation, because the speed of charges transfering increases linearly with the speed of rotation (Figure 6f-g and Figure S4, Support information). Generally, the amount of transferred charges is independent of the rotational speed of the TEHNG and usually remains constant, however, due to the slight instability of the water pressure, the rotor of the TEHNG can obtain greater rotational torque, and as the rotational speed and rotational torque increase, the TEHNG will get more large voltage and current output. In practical applications, high output power is usually obtained by combining TEHNG with matching resistance. Therefore, under different water pressure conditions, the performance of the TEHNG process can be improved by matching the best performance under different anti-external load modes. As shown in Figure 6h and Figure S5, when the water pressure is 0.35 MPa, the output current of TEHNG decreases with the increase of load resistance, and the output power gradually increases and then decreases. When the load resistance is set to $10^5$ Ω, the maximum peak power is 6 mW. With the increase of water pressure, TEHNG will get greater electrical output performance of voltage, current and power, which also becomes a potential energy harvesting device for high pressure fluid pipelines. Figure 6i illustrates the charging voltage curves of different specifications of commercial capacitors powered by the TEHNG unit under 0.35 MPa water pressure, with the increase of capacitor specifications, the charging time to reach the maximum voltage of the capacitor gradually becomes longer. The maximum voltage reached by the capacitor is 9 V, the 15 nF capacitor needs 10 s to charge to 9 V, and the 100 nF capacitor needs 25 s to charge to 9 V. For the hybrid NG module, the EMG component is the main contributor to electricity generation in the early stage of charging, while the TENGs component provides more and more electricity in the relatively late charging stage. After a certain time, the TEHNG can charge the capacitor to the maximum voltage, proving the best charging performance of the proposed hybrid NG.

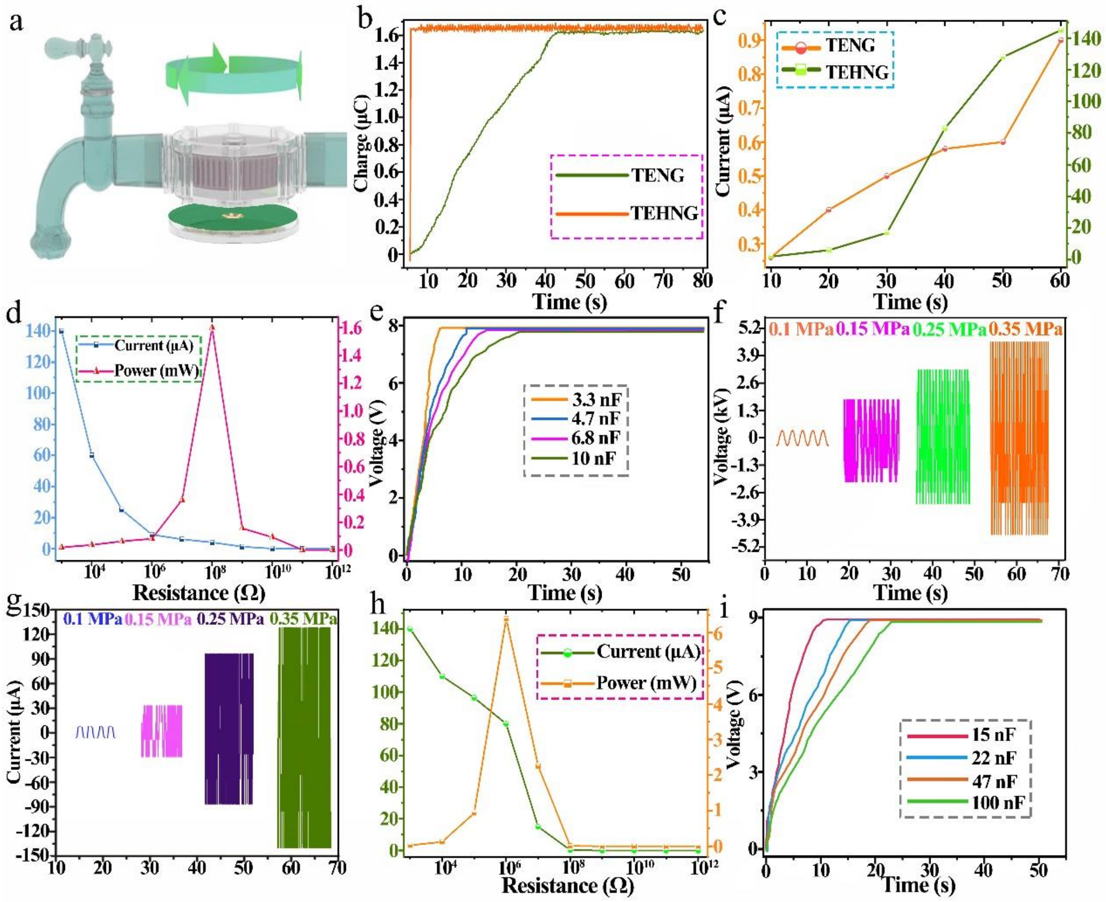


**Figure 6.** Schematic diagram of TEHNG, application and its electrical output performance. **a)** Schematic diagram of TEHNG installed in the pipeline. **b)** Comparison of charge transfer amount between TENGs and TEHNG. **c)** Comparison of current between TENGs and TEHNG. **d)** TEHNG output power at 1200 rpm. **e)** TEHNG charging performance of different capacitors. **f-g)** Voltage and current output performance of TEHNG under different water pressures. **h)** Output power performance of TEHNG under 0.35 MPa water pressure. **i)** TEHNG charging performance of different capacitors under 0.35 MPa water pressure.

To demonstrate the output performance of TEHNG in practical applications, some practical application performances are shown in this paper, and the corresponding circuit diagram is shown in Figure 7a, where EMG and TENGs are connected with a 100 nF capacitor through a full-wave rectifier. EMG and TENGs form TEHNG in parallel, which helps to increase the output current, because the total output current is equal to the sum of the two currents when the two modules are connected in parallel. In addition, EMG and TENGs are respectively connected to the load through a full-bridge rectifier, so that TEHNG has a more stable electrical output. When the switch is closed, the dual-mode TENGs can power the load and charge the capacitor through the full-bridge rectifier. Changes in the industrial production environment have a significant impact on the operation of the factory, so it is very necessary to monitor some parameters of the industrial production environment, and high-altitude operations or harsh field environments will bring great difficulties to installation and monitoring. Therefore, TEHNG is very to a large extent, the difficulties caused by this problem have been solved, and it has played an important role in the construction of an environmental monitoring system. In addition, commercial LEDs are used to detect the effectiveness of the electrical output performance of TEHNG. Here, TEHNG is used as the commercial LED function, and at least 512 LEDs are lit and TEHNG can output kV-level AC voltage, enough to continuously light up LEDs, as shown in Figure 7b. Figure 7c and e is a photo of low-power electronic devices powered by TEHNG, such as electronic watches, temperature and humidity detectors, and these low-power detection devices powered by TEHNG are valuable applications. Here we also tested the voltage validity of the electronic equipment, which is divided into three stages. When there is no fluid flowing in the pipeline, the voltage of the electronic equipment is 0 V. When there is fluid flowing, the voltage reaches 2.96 V, and then the value of the voltage is down to

0 V (Figure 7d). To demonstrate the power effect of TEHNG in practical applications, as shown in Figure 7f, the hybrid NG can continuously light the white ball lamp, in which a 47 μF capacitor is used to connect the nanogenerator and the white ball lamp. The mechanical energy $E_T$ of the water flow can be calculated by Bernoulli's equation:

$$E_T = gz + \frac{v^2}{2} + \frac{P_1}{\rho} + W_e \tag{3}$$

where $g$ is gravitational acceleration, $z$ is location head, $v$ is speed of water, $P$ is water pressure, $\rho$ is water density and $W_e$ is additional input energy. The formula for calculating electrical energy is as follows:

$$\mathrm{W} = \int_0^{\mathrm{T}} I_t^2 R\, dt \tag{4}$$

where $T$ is the running duration of the TEHNG and $I_t$ is current flowing through resistor. The converted electric energy of TEHNG at the maximum power consumption at one time is obtained by the following formula:

$$\textit{Energy conversion efficiency } (\eta) = \textit{Electrical energy/Mechanical energy} \tag{5}$$

Finally converted 0.23 J of total electrical energy at 1.01% efficiency. Under the driving function of the hybrid NG motor, the incandescent lamp has stable and sufficient brightness, and there will be no phenomenon of flashing off or discontinuous brightness. In addition, after 3000 friction cycles, it has slight fluctuations, but the stability is still excellent and the durability is reliable, which is attributed to the friction electrode structure and the structural characteristics of the soft contact (Figure S6).

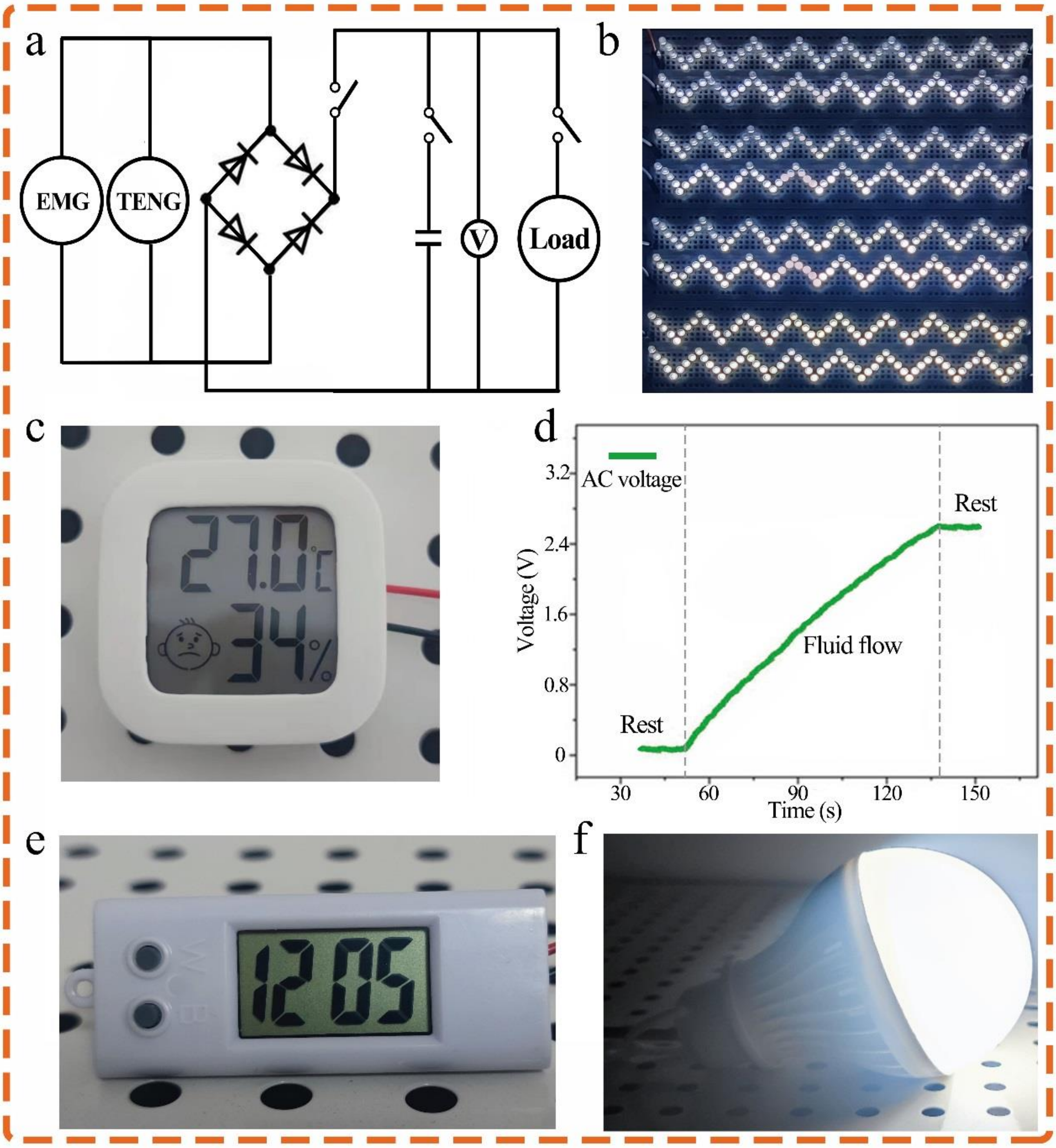


**Figure 7.** Application of TEHNG. **a)** TEHNG application circuit and its working principle. **b)** Photo of TEHNG lighting application. **c, e)** Photographs of the operating temperature sensor and electronic watch sensor, powered by TEHNG. **d)** Voltage variation of temperature monitoring device operation. **f)** Photograph of 512 LEDs lit in series powered by TEHNG.

## 3. Conclusions

In this work, a self-powered system based on a triboelectric-electromagnetic hybrid pipeline energy harvesting module is demonstrated. Rabbit fur and PTFE are used as triboelectric electrodes to fabricate disk-type soft-contact TENGs instead of traditional direct-contact TENGs to collect mechanical energy of fluid flow and convert it into electrical energy. The special structural design enables the two parts of each energy collection unit to effectively collect and convert the mechanical energy of the fluid in the equipment into electrical energy under the promotion of external mechanical energy, and supply energy for some low-power data monitoring devices. In this study, due to the addition of EMG, the output current and power of the hybrid generator has a significant enhancement compared with the TENGs module, the current is increased by 140 times, and the power is increased by three orders of magnitude. Especially through the new module, it is possible to simultaneously collect independent fluid energy and monitor data signals in harsh environments, such as the collection of fluid energy in industrial production pipelines and the monitoring of data such as temperature and humidity in the fluid environment. This work provides an efficient and sustainable advance for the practical application of fluid mechanical energy harvesting techniques and self-powered monitoring systems. And it provides an efficient strategy to simultaneously harvest multiple energies, significantly enhancing the output and facilitating the application of TENGs in engineering.

## 4. Experimental section

### 4.1 Fabrication of disk-type soft-contact TENGs module

The TENGs unit consists of two parts: rabbit fur and PTFE friction electrodes. For the fur part, glue four fan-shaped furs with the same sector to the acrylic sheet. The outer and inner diameters of the scalloped fur are 100 mm and 16 mm respectively. As a mature product, animal skins are readily available in the market at low prices. Here, we choose fur that integrates fur and skin, processed rabbit fur is about 10mm long, while wool, dog fur and fox fur are thicker (15-20 mm) and then use double-sided tape (3M LSE) and stick them on the acrylic support plate. For induction copper electrodes, epoxy fiberglass substrates (200 mm diameter) with copper layers (1 oz) were fabricated using PCB technology. The copper sector area of the PCB is divided into two groups, which are respectively connected to the load through wires. A 30 µm-thick PTFE film was then adhered to the copper layer as a tribodielectric layer via a conductive double-sided tape.

### 4.2 Manufacturing of water turbine

The EMG coils were prepared manually, the frame was 3D printed with ABS-A100 to arrange a neodymium magnet coil and nine copper coils, encapsulated in an ABS-A100 3D printed case with a diameter of 60 mm, the centers of the magnets and coils were placed in the diameter for a circumference of 21 mm.

### 4.3 Electrical measurement

The output electrical performance of the device was measured with a voltage preamplifier (Version Keithley 6517, impedance >200 TΩ, The Keithley. Inc., USA) and high voltage probe (Version HVP-40, 1:1000, The Pintech. Inc., China). The data acquisition and analysis platform consists of serial port direct connection RS-323 and LabVIEW 2020.

### 4.5 Water pressure and speed measurement

Water pressure multiplier for pressurization of pipeline fluid (KOMAX, Zhenyou E-Commerce Co., Ltd., China) and the tap water detection pressure gauge detects the pressure of the pipeline (Zhengxu Electronic Technology Co., Ltd., China). Delixi 827 tachometer (DLY-2301, Suning Tesco Group Co., Ltd., China) and commercial torque sensor (DYN-200, Yangge Technology Co., Ltd., China) to test the rotational speed of TENGs. The TENGs was driven by a DC motor (XD-37GB520, Shunyue Technology Co., Ltd., China).

## Declaration of competing interest

The authors declare that they have no known competing financial interests or personal relationships that could have appeared to influence the work reported in this paper.


## Acknowledgements

This work was supported by Fundamental Research Funds for the Central Universities (No.2572021BU06), Heilongjiang province postdoctoral funded project (LBH-Q21019 and LBH-Q21019), entrepreneurial practice project (202110225397), Donglin Green Biotechnology Co., Ltd, Heilongjiang. Natural Science Foundation (LH2020E087). The authors extend their appreciation to the Deanship of Scientific Research at King Khalid University for funding this work through under grant number (RGP. 2/106/43).


## References:


[1] Hill, D. J. 2008 Nuclear energy for the future *Nature Materials* **7** 680-682

[2] Cao, Y., Weng, M. M., Mahmoud, M. H. H., Elnaggar, A. Y., Zhang, L., El Azab, I. H., Chen, Y., Huang, M. N., Huang, J. T.,Sheng, X. X. 2022 Flame-retardant and leakage-proof phase change composites based on MXene/polyimide aerogels toward solar thermal energy harvesting *Adv. Compos. Hybrid Mater.* **5** 1253-1267

[3] Zhang, C. G., Liu, Y. B., Zhang, B. F., Yang, O., Yuan, W., He, L. X., Wei, X. L., Wang, J.,Wang, Z. L. 2021 Harvesting Wind Energy by a Triboelectric Nanogenerator for an Intelligent High-Speed

Train System *ACS Energy Lett.* **6** 1490-1499

[4] Ye, C. Y., Dong, K., An, J., Yi, J., Peng, X., Ning, C.,Wang, Z. L. 2021 A Triboelectric-Electromagnetic Hybrid Nanogenerator with Broadband Working Range for Wind Energy Harvesting and a Self-Powered Wind Speed Sensor *ACS Energy Lett.* **6** 1443-1452

[5] Yi, J., Dong, K., Shen, S., Jiang, Y., Peng, X., Ye, C. Y.,Wang, Z. L. 2021 Fully Fabric-Based Triboelectric Nanogenerators as Self-Powered Human-Machine Interactive Keyboards *Nano-Micro Lett.* **13** 13

[6] Wang, D. Y., Zhang, D. Z., Li, P., Yang, Z. M., Mi, Q. A.,Yu, L. D. 2021 Electrospinning of Flexible Poly(vinyl alcohol)/MXene Nanofiber-Based Humidity Sensor Self-Powered by Monolayer Molybdenum Diselenide Piezoelectric Nanogenerator *Nano-Micro Lett.* **13** 13

[7] Liu, H., Tang, J. W., Dong, L. Q., Wang, H., Xu, T. Y., Gao, W. C., Zhai, F., Feng, Y. Y.,Feng, W. 2021 Optically Triggered Synchronous Heat Release of Phase-Change Enthalpy and Photo-Thermal Energy in Phase-Change Materials at Low Temperatures *Advanced Functional Materials* **31** 11

[8] Liu, L., Guo, X. G.,Lee, C. 2021 Promoting smart cities into the 5G era with multi-field Internet of Things (IoT) applications powered with advanced mechanical energy harvesters *Nano Energy* **88** 36

[9] Ma, R., Cui, B., Hu, D. W., El-Bahy, S. M., Wang, Y., El Azab, I. H., Elnaggar, A. Y., Gu, H. X., Mersal, G. A. M., Huang, M. N.,Murugadoss, V. 2022 Enhanced energy storage of lead-free mixed oxide core double-shell barium strontium zirconate titanate@magnesium aluminate@zinc oxide-boron trioxide-silica ceramic nanocomposites *Adv. Compos. Hybrid Mater.* **5** 1477-1489

[10] Hui, Z., Xiao, M., Shen, D. Z., Feng, J. Y., Peng, P., Liu, Y. G., Duley, W. W.,Zhou, Y. N. 2020 A Self-Powered Nanogenerator for the Electrical Protection of Integrated Circuits from Trace Amounts of Liquid *Nano-Micro Lett.* **12** 9

[11] Fan, F. R., Tang, W.,Wang, Z. L. 2016 Flexible Nanogenerators for Energy Harvesting and Self-Powered Electronics *Adv. Mater.* **28** 4283-4305

[12] Chen, J., Zhu, G., Yang, W. Q., Jing, Q. S., Bai, P., Yang, Y., Hou, T. C.,Wang, Z. L. 2013 Harmonic-Resonator-Based Triboelectric Nanogenerator as a Sustainable Power Source and a Self-Powered Active Vibration Sensor *Adv. Mater.* **25** 6094-6099

[13] Qin, K., Chen, C., Pu, X. J., Tang, Q., He, W. C., Liu, Y. K., Zeng, Q. X., Liu, G. L., Guo, H. Y.,Hu, C. G. 2021 Magnetic Array Assisted Triboelectric Nanogenerator Sensor for Real-Time Gesture Interaction *Nano-Micro Lett.* **13** 9

[14] Liu, W. L., Wang, Z., Wang, G., Liu, G. L., Chen, J., Pu, X. J., Xi, Y., Wang, X., Guo, H. Y., Hu, C. G.,Wang, Z. L. 2019 Integrated charge excitation triboelectric nanogenerator *Nat. Commun.* **10** 9

[15] Xiong, J. Q., Cui, P., Chen, X. L., Wang, J. X., Parida, K., Lin, M. F.,Lee, P. S. 2018 Skin-touch-actuated textile-based triboelectric nanogenerator with black phosphorus for durable biomechanical energy harvesting *Nat. Commun.* **9** 9

[16] Wang, Z. L. 2020 Triboelectric Nanogenerator (TENG)-Sparking an Energy and Sensor Revolution *Advanced Energy Materials* **10** 6

[17] Jin, T., Sun, Z. D., Li, L., Zhang, Q., Zhu, M. L., Zhang, Z. X., Yuan, G. J., Chen, T., Tian, Y. Z., Hou, X. Y.,Lee, C. 2020 Triboelectric nanogenerator sensors for soft robotics aiming at digital twin applications *Nature Communications* **11** 12

[18] Zhou, Y. K., Shen, M. L., Cui, X., Shao, Y. C., Li, L. J.,Zhang, Y. 2021 Triboelectric nanogenerator based self-powered sensor for artificial intelligence *Nano Energy* **84** 12

[19] Khorsand, M., Tavakoli, J., Guan, H. W.,Tang, Y. H. 2020 Artificial intelligence enhanced mathematical modeling on rotary triboelectric nanogenerators under various kinematic and geometric conditions *Nano Energy* **75** 12

[20] Liu, Z. R., Nie, J. H., Miao, B., Li, J. D., Cui, Y. B., Wang, S., Zhang, X. D., Zhao, G. R., Deng, Y. B., Wu, Y. H., Li, Z., Li, L. L.,Wang, Z. L. 2019 Self-Powered Intracellular Drug Delivery by a Biomechanical Energy-Driven Triboelectric Nanogenerator *Advanced Materials* **31** 8

[21] Liang, X., Jiang, T., Liu, G. X., Feng, Y. W., Zhang, C.,Wang, Z. L. 2020 Spherical triboelectric nanogenerator integrated with power management module for harvesting multidirectional water wave energy *Energy Environ. Sci.* **13** 277-285

[22] Tao, K., Yi, H. P., Yang, Y., Chang, H. L., Wu, J., Tang, L. H., Yang, Z. S., Wang, N., Hu, L. X., Fu, Y. Q., Miao, J. M.,Yuan, W. Z. 2020 Origami-inspired electret-based triboelectric generator for biomechanical and ocean wave energy harvesting *Nano Energy* **67** 11

[23] Guan, Q. B., Dai, Y. H., Yang, Y. Q., Bi, X. Y., Wen, Z.,Pan, Y. 2018 Near-infrared irradiation induced remote and efficient self-healable triboelectric nanogenerator for potential implantable electronics *Nano Energy* **51** 333-339

[24] Pu, X., Li, L. X., Song, H. Q., Du, C. H., Zhao, Z. F., Jiang, C. Y., Cao, G. Z., Hu, W. G.,Wang, Z. L. 2015 A Self-Charging Power Unit by Integration of a Textile Triboelectric Nanogenerator and a Flexible Lithium-Ion Battery for Wearable Electronics *Advanced Materials* **27** 2472-2478

[25] Ma, Z. L., Xiang, X. L., Shao, L., Zhang, Y. L.,Gu, J. W. 2022 Multifunctional Wearable Silver Nanowire Decorated Leather Nanocomposites for Joule Heating, Electromagnetic Interference Shielding and Piezoresistive Sensing *Angew. Chem.-Int. Edit.* **61** 9

[26] Zhang, C., Zhou, T., Tang, W., Han, C. B., Zhang, L. M.,Wang, Z. L. 2014 Rotating-Disk-Based Direct-Current Triboelectric Nanogenerator *Advanced Energy Materials* **4** 7

[27] Dai, B., Ma, Y., Dong, F., Yu, J., Ma, M. L., Thabet, H. K., El-Bahy, S. M., Ibrahim, M. M., Huang, M. N., Seok, I., Roymahapatra, G., Naik, N., Xu, B. B., Ding, J. X.,Li, T. X. 2022 Overview of MXene and conducting polymer matrix composites for electromagnetic wave absorption *Adv. Compos. Hybrid Mater.* **5** 704-754

[28] Xie, Y. N., Wang, S. H., Lin, L., Jing, Q. S., Lin, Z. H., Niu, S. M., Wu, Z. Y.,Wang, Z. L. 2013 Rotary Triboelectric Nanogenerator Based on a Hybridized Mechanism for Harvesting Wind Energy *Acs Nano* **7** 7119-7125

[29] Pan, D., Yang, G., Abo-Dief, H. M., Dong, J. W., Su, F. M., Liu, C. T., Li, Y. F., Xu, B. B., Murugadoss, V., Naik, N., El-Bahy, S. M., El-Bahy, Z. M., Huang, M. A.,Guo, Z. H. 2022 Vertically Aligned Silicon Carbide Nanowires/ Boron Nitride Cellulose Aerogel Networks Enhanced Thermal Conductivity and Electromagnetic Absorbing of Epoxy Composites *Nano-Micro Lett.* **14** 19

[30] Zhao, Y. H., Liu, K. X., Hou, H.,Chen, L. Q. 2022 Role of interfacial energy anisotropy in dendrite orientation in Al-Zn alloys: A phase field study *Mater. Des.* **216** 14

[31] He, Y. X., Zhou, M. Y., Mahmoud, M. H. H., Lu, X. S., He, G. Y., Zhang, L., Huang, M. N., Elnaggar, A. Y., Lei, Q., Liu, H., Liu, C. T.,El Azab, I. H. Multifunctional wearable strain/pressure sensor based on conductive carbon nanotubes/silk nonwoven fabric with high durability and low detection limit *Adv. Compos. Hybrid Mater.* 12

[32] Gao, T., Rong, H. W., Mahmoud, K. H., Ruan, J. C., El-Bahy, S. M., Faheim, A. A., Li, Y. X., Huang, M. A., Nassan, M. A.,Zhao, R. Z. 2022 Iron/silicon carbide composites with tunable high-frequency magnetic and dielectric properties for potential electromagnetic wave absorption *Adv. Compos. Hybrid Mater.* **5** 1158-1167

[33] Liu, H., Wang, H. B., Lu, X. H., Murugadoss, V., Huang, M. N., Yang, H. S., Wan, F. X., Yu, D. G.,Guo, Z. H. 2022 Electrospun structural nanohybrids combining three composites for fast helicide delivery *Adv. Compos. Hybrid Mater.* **5** 1017-1029

[34] Song, W. Z., Wang, X. X., Qiu, H. J., Liu, Q., Zhang, J., Fan, Z. Y., Yu, M., Ramakrishna, S., Hu,

H.,Long, Y. Z. 2019 Sliding non-contact inductive nanogenerator *Nano Energy* **63** 9

[35] Wei, D., Weng, M. M., Mahmoud, M. H. H., Elnaggar, A. Y., El Azab, I. H., Sheng, X. X., Huang, M. N., El-Bahy, Z. M.,Huang, J. T. Development of novel biomass hybrid aerogel supported composite phase change materials with improved light-thermal conversion and thermal energy storage capacity *Adv. Compos. Hybrid Mater.* 12

[36] Fu, S. K., He, W. C., Tang, Q., Wang, Z., Liu, W. L., Li, Q. Y., Shan, C. C., Long, L., Hu, C. G.,Liu, H. 2022 An Ultrarobust and High-Performance Rotational Hydrodynamic Triboelectric Nanogenerator Enabled by Automatic Mode Switching and Charge Excitation *Advanced Materials* **34** 10

[37] Tan, D. J., Zeng, Q. X., Wang, X., Yuan, S. L., Luo, Y. L., Zhang, X. F., Tan, L. M., Hu, C. G.,Liu, G. L. 2022 Anti-Overturning Fully Symmetrical Triboelectric Nanogenerator Based on an Elliptic Cylindrical Structure for All-Weather Blue Energy Harvesting *Nano-Micro Lett.* **14** 12

[38] Pu, X., Song, W. X., Liu, M. M., Sun, C. W., Du, C. H., Jiang, C. Y., Huang, X., Zou, D. C., Hu, W. G.,Wang, Z. L. 2016 Wearable Power-Textiles by Integrating Fabric Triboelectric Nanogenerators and Fiber-Shaped Dye-Sensitized Solar Cells *Adv. Energy Mater.* **6** 9

[39] Chen, C., Wen, Z., Shi, J. H., Jian, X. H., Li, P. Y., Yeow, J. T. W.,Sun, X. H. 2020 Micro triboelectric ultrasonic device for acoustic energy transfer and signal communication *Nat. Commun.* **11** 9

[40] Zhou, L. L., Zhu, L. P., Yang, T., Hou, X. M., Du, Z. T., Cao, S., Wang, H. L., Chou, K. C.,Wang, Z. L. 2022 Ultra-Stable and Durable Piezoelectric Nanogenerator with All-Weather Service Capability Based on N Doped 4H-SiC Nanohole Arrays *Nano-Micro Lett.* **14** 10

[41] Xu, W. H., Zheng, H. X., Liu, Y., Zhou, X. F., Zhang, C., Song, Y. X., Deng, X., Leung, M., Yang, Z. B., Xu, R. X., Wang, Z. L., Zeng, X. C.,Wang, Z. K. 2020 A droplet-based electricity generator with high instantaneous power density *Nature* **578** 392-+

[42] Zhang, Y. L., Kong, J.,Gu, J. W. 2022 New generation electromagnetic materials: harvesting instead of dissipation solo *Sci. Bull.* **67** 1413-1415

[43] Gao, L. X., Lu, S., Xie, W. B., Chen, X., Wu, L. K., Wang, T. T., Wang, A. B., Yue, C. Q., Tong, D. Q., Lei, W. Q., Yu, H., He, X. B., Mu, X. J., Wang, Z. L.,Yang, Y. 2020 A self-powered and self-functional tracking system based on triboelectric-electromagnetic hybridized blue energy harvesting module *Nano Energy* **72** 11

[44] Kong, D. S., El-Bahy, Z. M., Algadi, H., Li, T., El-Bahy, S. M., Nassan, M. A., Li, J. R., Faheim, A. A., Li, A., Xu, C. X., Huang, M. N., Cui, D. P.,Wei, H. G. Highly sensitive strain sensors with wide operation range from strong MXene-composited polyvinyl alcohol/sodium carboxymethylcellulose double network hydrogel *Adv. Compos. Hybrid Mater.* 12

[45] Yang, H. M., Wang, M. F., Deng, M. M., Guo, H. Y., Zhang, W., Yang, H. K., Xi, Y., Li, X. G., Hu, C. G.,Wang, Z. L. 2019 A full-packaged rolling triboelectric-electromagnetic hybrid nanogenerator for energy harvesting and building up self-powered wireless systems *Nano Energy* **56** 300-306

[46] Feng, Y. W., Liang, X., An, J., Jiang, T.,Wang, Z. L. 2021 Soft-contact cylindrical triboelectric-electromagnetic hybrid nanogenerator based on swing structure for ultra-low frequency water wave energy harvesting *Nano Energy* **81** 8

[47] Wu, N. N., Zhao, B. B., Chen, X. Y., Hou, C. X., Huang, M. N., Alhadhrami, A., Mersal, G. A. M., Ibrahim, M. M.,Tian, J. 2022 Dielectric properties and electromagnetic simulation of molybdenum disulfide and ferric oxide-modified Ti3C2TX MXene hetero-structure for potential microwave absorption *Adv. Compos. Hybrid Mater.* **5** 1548-1556

[48] Zhong, X. D., Yang, Y., Wang, X.,Wang, Z. L. 2015 Rotating-disk-based hybridized electromagnetic-triboelectric nanogenerator for scavenging biomechanical energy as a mobile power source *Nano Energy* **13** 771-780

[49] Cho, H., Kim, I., Park, J.,Kim, D. 2022 A waterwheel hybrid generator with disk triboelectric nanogenerator and electromagnetic generator as a power source for an electrocoagulation system *Nano Energy* **95** 11

[50] Chen, X., Gao, L. X., Chen, J. F., Lu, S., Zhou, H., Wang, T. T., Wang, A. B., Zhang, Z. F., Guo, S. F., Mu, X. J., Wang, Z. L.,Yang, Y. 2020 A chaotic pendulum triboelectric-electromagnetic hybridized nanogenerator for wave energy scavenging and self-powered wireless sensing system *Nano Energy* **69** 10

[51] Zhang, B. S., Zhang, S., Li, W. B., Gao, Q., Zhao, D., Wang, Z. L.,Cheng, T. H. 2021 Self-Powered Sensing for Smart Agriculture by Electromagnetic-Triboelectric Hybrid Generator *ACS Nano* **15** 20278-20286

[52] Du, Y. Z., Wang, X. D., Dai, X. Y., Lu, W. X., Tang, Y. S.,Kong, J. 2022 Ultraflexible, highly efficient electromagnetic interference shielding, and self-healable triboelectric nanogenerator based on Ti 3 C 2 T x MXene for self-powered wearable electronics *J. Mater. Sci. Technol.* **100** 1-11

[53] Li, R. N., Wei, X. L., Shi, Y. P., Yuan, Z. H., Wang, B. C., Xu, J. H., Wang, L. F., Wu, Z. Y.,Wang, Z. L. 2022 Low-grade heat energy harvesting system based on the shape memory effect and hybrid triboelectric-electromagnetic nanogenerator *Nano Energy* **96** 10

[54] Zhang, Y., Zeng, Q. X., Wu, Y., Wu, J., Yuan, S. L., Tan, D. J., Hu, C. G.,Wang, X. 2020 An Ultra-Durable Windmill-Like Hybrid Nanogenerator for Steady and Efficient Harvesting of Low-Speed Wind Energy *Nano-Micro Lett.* **12** 11

[55] Li, H., Zhang, X., Zhao, L. M., Jiang, D. J., Xu, L. L., Liu, Z., Wu, Y. X., Hu, K., Zhang, M. R., Wang, J. X., Fan, Y. B.,Li, Z. 2020 A Hybrid Biofuel and Triboelectric Nanogenerator for Bioenergy Harvesting *Nano-Micro Lett.* **12** 12

[56] Tao, K., Chen, Z. S., Yi, H. P., Zhang, R. R., Shen, Q., Wu, J., Tang, L. H., Fan, K. Q., Fu, Y. Q., Miao, J. M.,Yuan, W. Z. 2021 Hierarchical Honeycomb-Structured Electret/Triboelectric Nanogenerator for Biomechanical and Morphing Wing Energy Harvesting *Nano-Micro Lett.* **13** 16

[57] Lee, D. W., Jeong, D. G., Kim, J. H., Kim, H. S., Murillo, G., Lee, G. H., Song, H. C.,Jung, J. H. 2020 Polarization-controlled PVDF-based hybrid nanogenerator for an effective vibrational energy harvesting from human foot *Nano Energy* **76** 9